Rock and Soil Mechanics

Volume 42 | Issue 5 Article 4

9-16-2021

Joint arrival-time picking method of microseismic P-wave and S-wave based on time-frequency analysis

Bao-xin JIA
Institute of Geology, China Earthquake Administration, Beijing 100029, China

Feng LI
School of Civil Engineering, Liaoning Technical University, Fuxin, Liaoning 123000, China

Lin-li ZHOU
School of Civil Engineering, Liaoning Technical University, Fuxin, Liaoning 123000, China

Shuai WANG
School of Civil Engineering, Liaoning Technical University, Fuxin, Liaoning 123000, China

See next page for additional authors

Custom Citation

JIA Bao-xin, LI Feng, ZHOU Lin-li, WANG Shuai, LIU Jia-shun, . Joint arrival-time picking method of microseismic P-wave and S-wave based on time-frequency analysis[J]. Rock and Soil Mechanics, 2021, 42(5): 1253-1265.

Joint arrival-time picking method of microseismic P-wave and S-wave based on time-frequency analysis

Authors

Bao-xin JIA, Feng LI, Lin-li ZHOU, Shuai WANG, and Jia-shun LIU

Rock and Soil Mechanics 2021 42(5): 1253−1265 ISSN 1000−7598
https: //doi.org/10.16285/j.rsm.2020.6439 rocksoilmech.researchcommons.org/journal

Joint arrival-time picking method of microseismic P-wave and S-wave based on time-frequency analysis

JIA Bao-xin[1, 2], LI Feng[1], ZHOU Lin-li[1], WANG Shuai[1], LIU Jia-shun[1]

1. School of Civil Engineering, Liaoning Technical University, Fuxin, Liaoning 123000, China

2. Institute of Geology, China Earthquake Administration, Beijing 100029, China

Abstract: Accurate acquisition of arrival time of microseismic signals is an important prerequisite for focal location, and the accurate acquisition of arrival time of P-wave and S-wave of microseismic signals has important theoretical significance. Based on the principles of time-frequency analysis and the arrival-time picking, the time-frequency analysis-downhill comparison method is proposed. According to the time-frequency analysis principle of this method, the position and rule of background noise, the frequency, amplitude and energy of microseismic signals before and after the initial arrival of P-wave and S-wave and smooth waveforms that facilitate the comparison of iterative averages can be obtained through spectrogram, power density spectrum and two successive FIR band-pass filters. By setting the mathematical expectation of the full wavelet amplitude as the threshold and iteratively comparing wavelet amplitudes of microseismic signals based on three relationships of power, arrival order and waveform overlap of P-wave and S-wave, the precise arrival time of P-wave and the arrival time of S-wave peak value are obtained. The advantages of this method over the improved STA/LTA method are compared by model tests and have been verified in an engineering example. The results show that: compared with the improved STA/LTA method, this proposed method can simultaneously pick up the precise arrival time of P-wave and the arrival time of S-wave peak value, while the latter can only pick up the accurate arrival time of P-wave. The average time difference and standard deviation of the former are 6.18 ‰ and 3.98 ‰ of the latter, respectively. Additionally, the average calculation time and standard deviation of the former are 43.99% and 10.54% of the latter, respectively. The failure ratio of the former is 0 while that of the latter is 15.63%.

Keywords: time-frequency analysis; FIR band-pass filtering; time acquisition of P-wave and S-wave; TFA-DC method; improved STA/LTA method

1 Introduction

With the continuous development of the economy, the demand for mineral resources in China is rapidly increasing. The mining and supply of mineral resources have brought economic benefits to our country, which is also accompanied by some environmental and safety hazards such as rib spalling and roof falling of roadway, rock burst, and goaf collapse[1−4]. As a new type of monitoring method, microseismic monitoring uses the geophone with a high sample rate to receive microseismic signals generated by rock mass deformation in real time, extract the initial arrival time of microseismic signals, and invert the location of the seismic source and the time of occurrence. Then the rock interface damage, matrix or inclusion fracture can be predicted and monitored during the mining process, which can further ensure construction safety and reduce economic losses. At present, the accuracy of inversion of the seismic source location and the occurrence time mainly depends on the accuracy of arrival-time picking and the wave velocity model[5−6].

The algorithm of automatically arrival-time picking of microseismic signals is mainly premised on the properties of the signal in terms of energy, frequency, travel time, and waveform[7]. Currently, researchers usually improve the accuracy of arrival-time picking by integrating or improving traditional arrival-time picking methods, which can contribute to the accurate inversion of seismic source location. Ross et al.[8] determined the P-wave arrival picking and first-motion polarity with deep learning. Based on the convolutional neural network, Perol et al.[9] proposed a method for detection and arrival-time picking of earthquakes. Moreover, Lee et al.[10] developed a modified energy ratio method (MER) for accurate arrival-time picking. Using the method of phase arrival identification-kurtosis (PAI-k) and the criterion of most frequency value (MFV), an improved algorithm PAI-k-MFV was proposed by Zhu et al.[11]. According to Hilbert-Huang transform (HHT) and Akaike information criterion (AIC), the HHT-AIC method for detection and arrival-time picking of earthquakes was established by Jia et al.[12]. Additionally, a S-wave phase picking method with four indicators of three functions for microseismic signals was put forward by Zhang et al.[7]. Based on the method of short time-window average/long time- window average (STA/LTA), the polarization method and the AIC criterion, a hybrid algorithm STA/LTA- Polarization-AIC for arrival-time picking of P-wave was proposed by Diehl et al.[13].

Received: 22 Septembr 2020 Revised: 25 December 2020
This work was supported by the National Natural Science Foundation of China (51774173) and the Discipline Innovation Team of Liaoning Technical University (LNTU20TD08).
First author: JIA Bao-xin, male, born in 1978, PhD, Professor, mainly focusing on the investigation of mine disaster mechanics. E-mail: jbx_811010@126.com

What's more, an algorithm Kurtosis-AIC on the basis of the AIC value of kurtosis curve was developed by Zhao et al.[14]. Furthermore, Zhang et al.[15] proposed a hybrid ZTR algorithm according to discrete wavelet transform (DWT) and the AIC criterion.

The above research results have greatly improved the accuracy of positioning to a certain extent. However, with the increase in the layout density of the geophones[16-17], the quality difference between the waveforms collected by different geophones has become larger and larger. Therefore, even if the picking method with high accuracy is adopted, there will be a large error in the picking result for some signals with poor quality, which leads to an increase in the error for the seismic source inversion. The error is particularly large for waveforms with insignificant time difference and low signal-to-noise ratio. Furthermore, the accuracy and stability of arrival-time picking results using the methods mentioned above are insufficient, and it is difficult for the picking results to reach the ms level. Moreover, abrupt changes can be observed in picking results, resulting in high dispersion.

To solve these problems, the position and rule of background noise, the frequency, amplitude and energy of microseismic signals before and after the initial arrival of P-wave and S-wave and smooth waveforms can be obtained by analyzing spectrogram, and power density spectrum. Additionally, the dominant frequency of S-wave is used as the center point, and the specified filtering range is used as the radius. Then two successive FIR band-pass filterings are performed to filter out regular background noises of high and low frequency whose power is greater than P-wave and S-wave signals. Afterwards, the dominant frequency of S-wave in the power density spectrum is clearly displayed, and the signal image is smoother, which is more suitable for iterative comparison. By setting the mathematical expectation of the full wavelet amplitude as the threshold and following three relationships of power, arrival order and waveform overlap of P-wave and S-wave, the time-frequency analysis-downhill comparison method is proposed.

2 Time-frequency analysis principle of the TFA-DC method

The principle of time-frequency analysis is the first theoretical basis of the TFA-DC method. Through spectrogram, power density spectrum and two successive FIR band-pass filterings, the frequency, amplitude and energy of microseismic signals before and after the initial arrival of P-wave and S-wave and smooth waveforms that facilitate the comparison of iterative averages can be obtained to iteratively compare the amplitude of the subsequent wavelets.

2.1 Spectrogram analysis

The spectrogram is drawn based on the short-time Fourier transform (STFT), which is often used in the analysis of the spectrum of the response signal under the excitation of slow time-varying signals and dynamic load. The frequency-domain characteristics of the signal $h(t)$ at a certain time t can be strengthened by multiplying the window function $w(t)$ centered on τ and the signal together, and then the signal at the other moment can be weakened. The STFT can be defined as[18]

$$\mathrm{STFT}(t,f)=\int_{-\infty}^{\infty}h(\tau)\cdot w(t-\tau)\mathrm{e}^{-2\pi ift}\mathrm{d}\tau \quad (1)$$

where h is the signal; τ is the time (s); f is the frequency (Hz); $\mathrm{STFT}(t,f)$ is the power of signal at time t with the frequency of f; and i is the imaginary unit.

According to the spectrogram, the initial arrival time of the microseismic signal and the power distribution of the mechanical vibration in each frequency range of the signal can be obtained. However, it is difficult to find the precise frequency and time due to the limited resolution of the spectrogram. If the resolution of the spectrogram is improved, the required access space and calculation time will greatly increase, making it difficult to provide real-time signal analysis results. Although the spectrogram can be used to find the approximate time and frequency distribution of the arrival of the microseismic signal, its accuracy is not sufficient for the inversion calculation of the seismic source. Therefore, further filtering and analysis of the power density spectrum are necessary.

2.2 Analysis of power density spectrum

The periodic power density spectrum is an estimation method for analyzing the power spectral density of the signal, which is suitable for response analysis under random dynamic load. The non-parametric spectrum estimation method with the generalized fixed random process is applied. For the signal collected at the device default sampling rate per unit time x_n, the estimation of the power spectrum is defined by this method[19] as

$$\hat{P}(f)=\frac{\Delta t}{N}\left|\sum_{n=0}^{N-1}x_n\mathrm{e}^{-\mathrm{i}2\pi f\Delta tn}\right|^2,\ -1/2\Delta t<f\leqslant 2\Delta t \quad (2)$$

where $\hat{P}(f)$ is the power spectrum estimation (dB/Hz); Δt is the sample interval (s); N is the sequence length; x_n is the signal collected at the device default sampling rate per unit time; and n is the sequence number of the signal collected per unit time.

The power density corresponding to each frequency band can be obtained from the power density spectrum. However, if we want to acquire the power densities of the P-wave and S-wave in the power density spectrum, the FIR band-pass filtering should be performed for the original data to eliminate the interference of background noise and unwanted signals.

2.3 Two successive FIR band-pass filterings

The band-pass filtering using non-recursive filters (FIR) is a common method for signal processing. Waves within the specific frequency band are allowed to pass in this method, while signals within other frequency ranges are attenuated to a very low level.

Two successive FIR band-pass filterings are performed for original signals in this study. The first one is rough filtering, which can filter out regular high-frequency and low-frequency background noise with power greater than those of P-wave and S-wave signals.

Therefore, the dominant frequency of S-wave in the power density spectrum is clearly displayed. The second one is accurate filtering, which can filter out most of the unwanted signals. Then only the signals within the accurate filtering radius R (Hz) are processed. Hence, the required bandwidth can be accurately selected, and the signal image is smoother, which is more suitable for iterative comparison. The two filtering methods are described as below.

2.3.1 Rough filtering

There is always background noise with regular changes and high power in the actual microseismic signal. To eliminate the effect of background noise on the extraction of power of the S-wave dominant frequency and peak arrival time, the upper frequency limit of low-frequency background noise and the lower frequency limit of high-frequency background noise are selected as the filtering range of rough filtering.

The frequency band of high-frequency background noise is often above 1 kHz, while the frequencies of P-wave and S-wave in microseismic signals are rarely larger than 1 kHz. Therefore, 1 kHz is directly chosen as the upper limit of rough filtering to improve the calculation speed. The lower limit of rough filtering is the upper limit of low-frequency background noise whose power is greater than those of P-wave and S-wave. Therefore, the corresponding power averages for a certain segment of background noise should be iteratively compared from low to high frequencies to determine the inflection point of the power attenuation of the low-frequency background noise. As a result, the lower limit of rough filtering can also be determined. The steps are as follows:

(1) Suppose the time corresponding to the maximum amplitude in the original signal is T.

(2) Capture the signal from (T–1.5) s to (T–1) s.

(3) Process the power density spectrum of the signal to obtain the frequency distribution F and the corresponding power distribution P.

(4) Suppose the initial value of i is 1, the value of β is 2, and the iteration factors D_1 and D_2 satisfy the following relationship:

$$D_1 = \frac{P_{1+(i-1)\beta} + P_{2+(i-1)\beta} + \cdots + P_{i\beta}}{\beta} \tag{3}$$

$$D_2 = \frac{P_{1+i\beta} + P_{2+i\beta} + \cdots + P_{(i+1)\beta}}{\beta} \tag{4}$$

where P_i is the i-th element of the power distribution P, and β is the number of elements to obtain the mathematic expectation.

(5) Compare D_1 and D_2. If $D_1 < D_2$, output the $(1+i\beta)$ th element of F as the lower limit of rough filtering. Otherwise, reset i to $i+1$ and execute step (5).

2.3.2 Accurate filtering

The frequency corresponding to the maximum power in the power density spectrum of the rough filtering is selected as the origin of accurate filtering with the radius of accurate filtering R, and the band-pass filtering is executed on the signal after rough filtering. When the dominant frequencies of P-wave and S-wave are close to each other, R can be set smaller. On the contrary, a larger value can be chosen for R when the dominant frequencies of P-wave and S-wave are different from each other. In actual application, the dominant frequencies of P-wave and S-wave change within a certain range, and their bandwidths are much greater than 1 Hz. Therefore, their information can be included in accurate filtering as long as the selection of R does not exceed the intersection range of their frequency bands. Then the value of R does not need to be too precise, which can be set to be 1, 10, 100 Hz, etc. according to the magnitude of the difference between the dominant frequencies of P-wave and S-wave. The smaller the R, the more accurate the filtering; the larger the R, the more details the signal retains.

3 Arrival-time picking principle of the TFA-DC method

The arrival-time picking principle is the 2nd theoretical basis of the TFA-DC method. After the result of the time-frequency analysis is obtained, the arrival time of P-wave and S-wave can be picked according to the three relationships of P-wave and S-wave. These three relationships include power, arrival order and waveform overlap. The distributions of P-wave and S-wave in the filtered signals are determined according to the power level based on the arrival-time picking principle. Then the arrival time of S-wave peak can be found by comparing the wavelet amplitudes, and finally the accurate arrival time of P-wave is acquired by iterating towards the left according to the position of the arrival time of S-wave peak.

3.1 Connection between P-wave and S-wave

After analyzing the original signal spectrogram and power density spectrum, and performing two successive FIR band-pass filterings, three relationships of P-wave and S-wave are as follows: power, arrival order, and waveform overlap.

3.1.1 Power

The power and amplitude of S-wave in the microseismic signal are greater than those of P-wave[20]. The surge in amplitude induced by the initial arrival of the microseismic signal is mainly caused by the arrival of S-wave. Therefore, the picking of the seismic phase by S-wave is more concise than P-wave.

3.1.2 Arrival order

In most cases, the velocity of P-wave is greater than the velocity of S-wave, so P-wave can reach the geophone before S-wave. According to the waveform of the microseismic signal, the sudden change in the microseismic signal waveform caused by the arrival of P-wave should be located on the left side of that caused by the arrival of S-wave.

3.1.3 Waveform overlap

Generally, the distance between the seismic source location and the geophone is relatively small. There-

fore, the mechanical vibration caused by the initial arrival of P-wave cannot completely calm down before the arrival of S-wave, which can result in overlap of the waveforms of S-wave and P-wave[21] as shown in Fig.1.

In summary, it is necessary to find the arrival time of S-wave peak before picking the accurate arrival time of P-wave. However, the accurate time information of S-wave is often concealed by tail of P-wave and background noise. Thus, the arrival time of the peak value of S-wave is first extracted to improve the adaptability of the algorithm and the calculation speed of the algorithm.

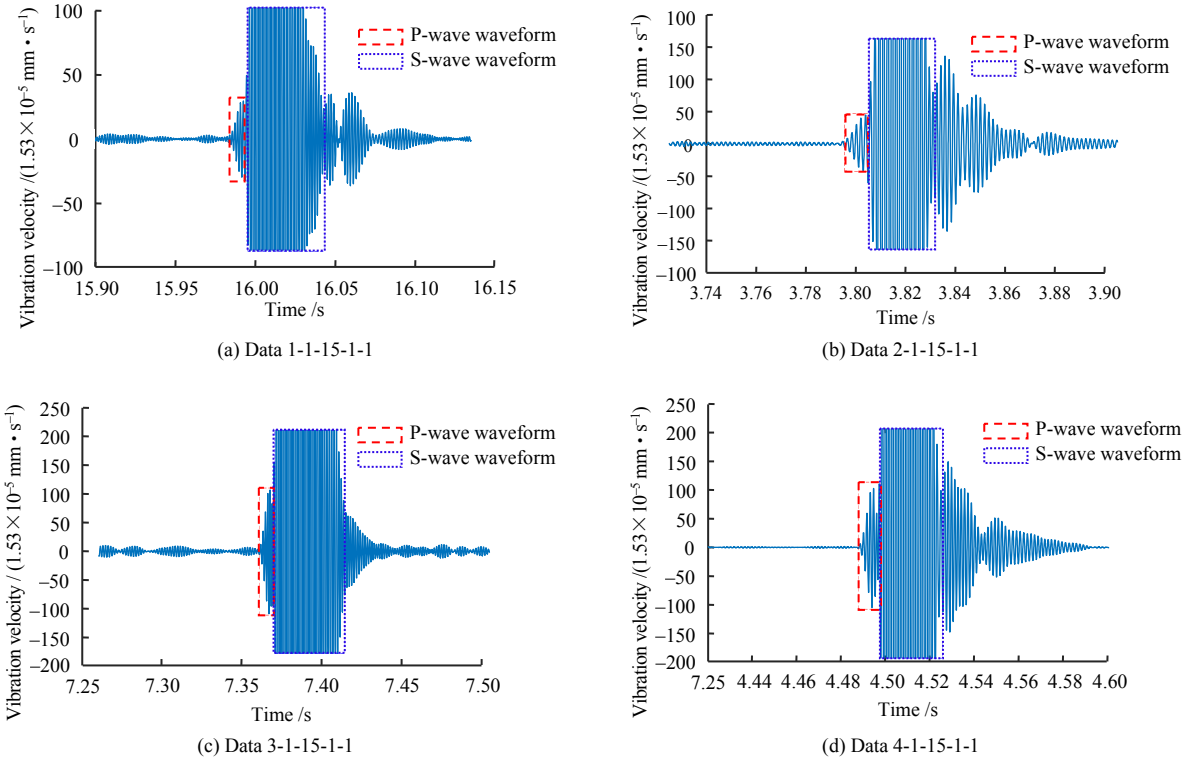

(a) Data 1-1-15-1-1 (b) Data 2-1-15-1-1

(c) Data 3-1-15-1-1 (d) Data 4-1-15-1-1

Fig. 1 Overlap of P-wave and S-wave

3.2 Arrival-time picking of the peak value of S-wave

According to the above analysis, the arrival time of the peak value of S-wave in the signal after the accurate filtering corresponds to time of the first maximum point of the signal wavelet amplitude after the accurate arrival time of P-wave. Based on the law of conservation of energy, the amplitude of the mechanical vibration of the geophone should gradually decrease after the arrival of S-wave. In other words, the amplitude of the signal wavelet should gradually decrease, and there will be no repeated oscillations of the signal wavelet amplitude after the arrival of S-wave signal. Consequently, the arrival time of the peak value of S-wave should be the time corresponding to the maximum amplitude of the signal wavelet after the accurate arrival time of P-wave. Because the amplitude of the signal wavelet itself is the maximum value of the current wavelet, the arrival time of the peak value of S-wave can be gained by sorting all sample values of the signal by size.

3.3 Accurate arrival-time picking of P-wave

In order to obtain the accurate arrival time of P-wave, the iterative comparison method is used to sequentially compare the amplitude at the arrival time of S-wave peak with the wavelet amplitude on the left side of the signal. The flow chart is shown in Fig.2, and the steps for this method are as follows.

3.3.1 Signal wavelet amplitude picking

The signal wavelet amplitude can be extracted using the findpeaks function in the Matlab software. The number of the amplitude picking can be controlled by setting the picking interval of amplitude Q reasonably. The picking interval of amplitude Q satisfies the following formula:

$$Q = \left\lfloor \frac{S}{f_S} \right\rfloor \tag{5}$$

where Q is the minimum picking interval of amplitude; S is the total number of sample points, and f_S is the device default sampling frequency (Hz).

All wavelet amplitudes of the signal after the accurate filtering can be found out using this method as shown in Fig.3.

3.3.2 Threshold selection for iterative comparison

The mathematical expectation k of all wavelet amplitudes of the signal after the accurate filtering is set as the threshold. This value is much smaller than the amplitude corresponding to the arrival time of S-wave peak, so the iteration will not end early due to a large allowable range of the threshold. Additionally, this threshold is also smaller than the amplitude corresponding to the vibration caused by P-wave and other unexpected signals. Therefore, this ensures that

the iteration factor can cross the minimum value between the amplitude corresponding to the arrival time of S-wave peak and the amplitude corresponding to the accurate arrival time of P-wave, which can further help the iteration factor reach the value of stable vibration on the left side of P-wave.

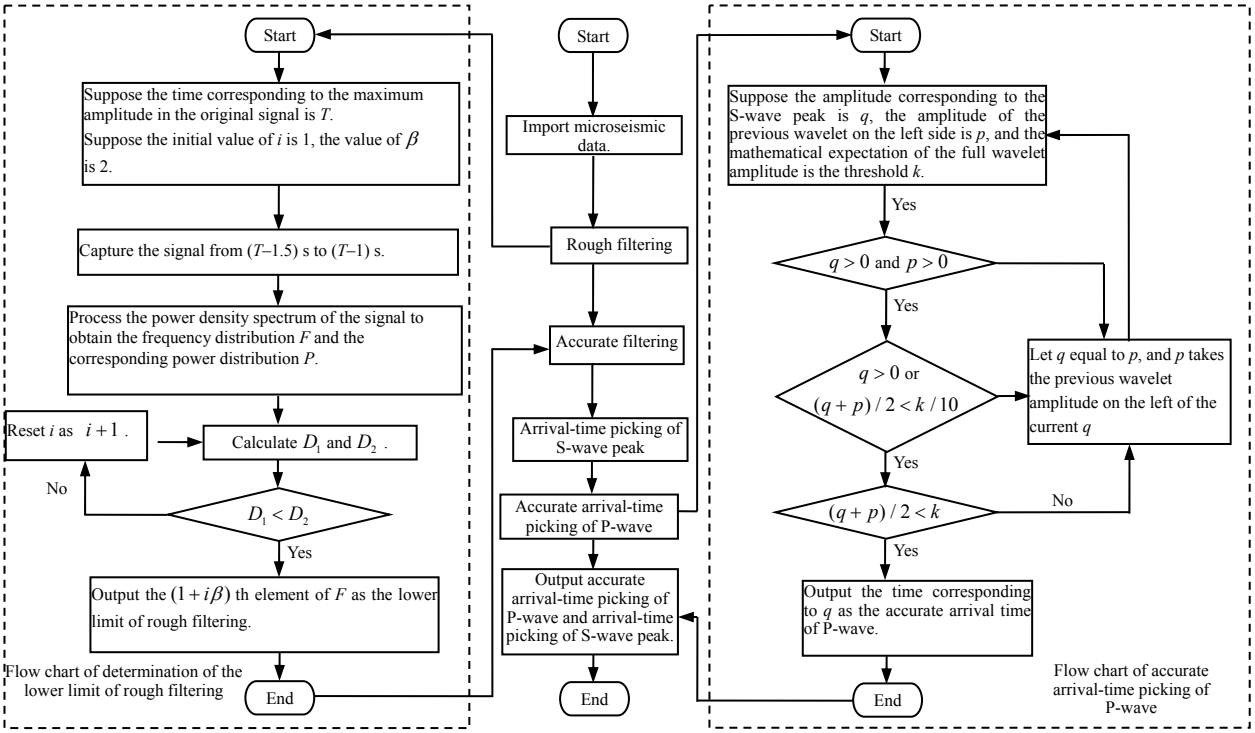

Fig. 2 Flow chart of TFA-DC method

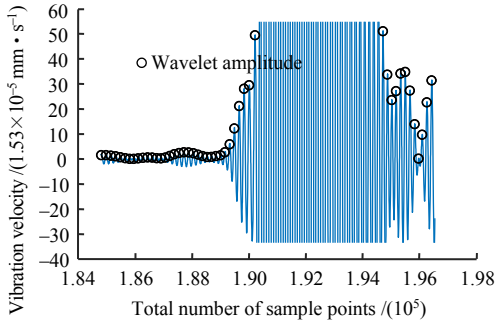

Fig. 3 Full wavelet amplitude pick-up

The amplitude after the amplitude surge caused by the arrival of P-wave and S-wave is added to the mathematical expectation of the full wavelet amplitude, which can ensure that the threshold value is not too small. Furthermore, this can help the iteration factor not exceed the evaluated value because of the small threshold and help it continue to iterate to the left.

To make sure of the uniformity of the evaluation criteria of the threshold k, the two points should be followed: the first is to ensure that the duration of the microseismic signal that contains the arrival of P-wave and S-wave is the same; the second is to ensure that the background noise signal is basically the same in each single microseismic signal. The first point can ensure that the duration of each single microseismic signal is the same. The second point can make sure that there is no other strong background noise during the laboratory test. The travel time of P-wave and S-wave is usually measured in the unit of second in engineering. When the distances between the geo- phones are close and the layout environment is roughly the same, the background noise can be basically the same. When the geophones are far apart, it is also necessary to ensure that the working conditions around the geophones are basically the same.

3.3.3 Iteration steps

(1) Suppose the amplitude corresponding to the S-wave peak is q, the amplitude of the previous wavelet on the left side is p, and the mathematical expectation of the full wavelet amplitude is the threshold k.

(2) If both q and p are greater than 0, execute step (3).

(3) Compare q and p. If $q < p$ or the absolute value of the difference between q and p is smaller than $k/10$, execute step (4). Otherwise, execute the next iteration.

(4) Compare k and $(q+p)/2$. If k is larger than $(q+p)/2$, output the time corresponding to q as the accurate arrival time of P-wave. Otherwise, execute the next iteration.

(5) In the next iteration, q is reset to the current value of p, and the value of p is reset to the previous wavelet amplitude on the left of the current p. Execute step (2).

4 Model test and case analysis

In order to verify the time-frequency analysis principle, the calculation speed, the accuracy of the picking results, the adaptability of the signal with a

low signal-to-noise ratio and the stability of the picking results in the TFA-DC method, a model is built in the laboratory and the geophones are installed. The results of the above problems are investigated by analyzing and comparing the microseismic signals generated by the pendulum impact.

4.1 Establishment of model test

4.1.1 Model establishment

The test model has a length of 3 m, a width of 0.3 m, and a height of 1.6 m. It is made of sand, lime, gypsum, and water mixed and stacked in layers, with a ratio of about 25:3:5:4. Nine geophones are embedded in the wall from the rear during the piling. After the model stacking is completed, the four chambers are excavated with tools and run through the whole wall. In Fig.4, the red cylinders represent the geophone, the yellow solid circles represent the impact position, and the blue cuboids represent the excavation chamber. These can be used to simulate the real underground environment and produce interference to the signal.

4.1.2 Monitoring device

In this test, an ultra-high frequency(UHF) multi-channel tectonic activity monitor (Antenna-III) with a sample frequency of 100 kHz and a monitorable band-width of 0-50 kHz is used to capture the unidirectional mechanical vibration signal of the pendulum impact.

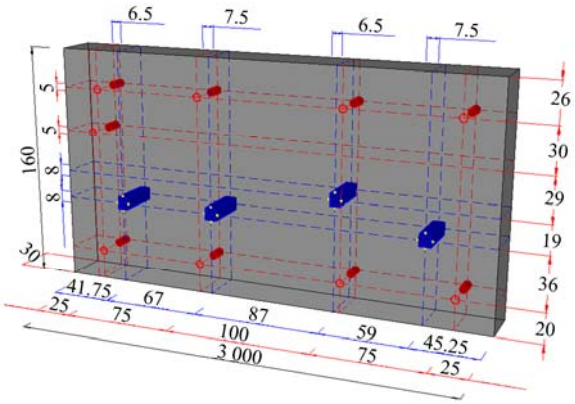

Fig. 4 Test layout (unit: cm)

Table 1 Parameters of the UHF multichannel tectonic activity monitor

Host hardware configuration			Geophone parameter			
CPU	RAM	Hard disk	Sample frequency /kHz	Vibration wave velocity range /(1.53×10^{-5} mm • s^{-1})	Number of geophone	Sensitivity /(V • s • m^{-1})
Core i7-2620M 2.7GHz	DDDR-III 4GB	SATA-III 2TB	100	–32 768～32 767	48	100

Z1—Pressure-sensitive touch screen；Z2—External I/O interface；Z3—Indicator for host running and hard disk working；L1—Host start switch (contact-point)；L2—Host power switch（self-lock）；L3—12V DC power interface；B1—Power supply instructions；B2—Screw hole on the heat sink

Fig. 5 UHF multichannel tectonic activity monitor

4.1.3 Test process

During the test, a single pendulum with a steel ball of a fixed length is used to hit the wall. The connecting line of the steel ball is flexible with a length of 70 cm, and the radius of the steel ball is 1 cm.

(1) Impact position: There are 16 impact locations in total with four in each chamber. For each chamber, the impact position is 1 cm from the midpoint of the upper edge of the chamber, 1 cm from the midpoint of the lower edge, 1 cm from the midpoint of the left edge, and 1 cm from the midpoint of the right edge.

(2) Impact mode: Firstly, direct the steel ball at the position to be hit. Then make it hang naturally and just touch the wall. Pull the steel ball to a certain distance perpendicular to the wall and let it go. Let the ball fall freely and hit the wall. Impact on each position for three times, with the impacting distance of 10, 15, 20, and 25 cm, respectively. The photo of the test site is displayed in Fig.6.

(3) Data collection: Turn on the UHF multichannel tectonic activity monitor before each impact. After the three impacts are completed, turn off the monitor and export the microseismic signal to the computer. The naming format of data is as follows: the first digit is the series number of chamber; the second digit is the impact position (one to four indicate left, right, upper, lower, respectively); the third digit denotes the lift height of the pendulum; the fourth digit denotes the series number of geophone; and the fifth digit denotes the order of the pendulum impact.

Fig. 6 Test site

4.2 Example analysis of the TFA-DC method

The Matlab software is used to analyze the test signal. The data used in the following example analysis is 1-1-15-1-1.

4.2.1 Original signal analysis of data 1-1-15-1-1

The original signal diagram of data 1-1-15-1-1 is shown in Fig.7. A violent change in the amplitude and the signal frequency can be observed around 16.0 s. According to the record of the impact time of the pendulum, it can be determined that this is the arrival point of the microseismic signal. The approximate arrival time of P-wave and S-wave at this point can be found by performing the time-frequency analysis on this point.

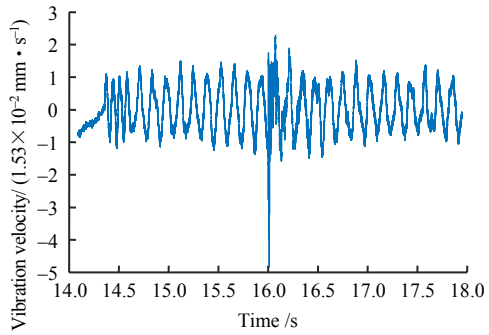

Fig. 7 Original signal diagram of data 1-1-15-1-1

4.2.2 Spectrogram analysis

The spectrogram of the original signal of data 1-1-15-1-1 is shown in Fig.8. By comparing Fig.7 and Fig.8, it is found that the signal breaks out of the original vibration period and begins to vibrate violently at around 16.0 s in Fig.7, and this point coincides with the point of maximum power in Fig.8. According to this, a violent change in the wide-band signal vibration can be witnessed at about 16.0 s within the frequency range from 220 to 1 300 Hz. The frequency of the maximum power corresponding to the violent change of this signal is the dominant frequency of S-wave because the power of S-wave is greater than that of P-wave. According to Fig.8, the power of this violent change reaches its maximum when the frequency is about 600 Hz. Therefore, the dominant frequency of S-wave is about 600 Hz. Additionally, the point of the maximum power corresponding to the dominant frequency of P-wave is basically distributed at about 590 Hz when checking from the point of the maximum power of the signal to its left. However, this value is slightly smaller than the maximum power of the signal. Thus, it can be judged that the dominant frequency of P-wave is approximately 590 Hz. After a large amount of calculation, the wave velocities of P-wave and S-wave are both within the range from 200 to 400 m/s, and the wave velocity of P-wave is slightly faster than that of S-wave. Moreover, the wavelengths of P-wave and S-wave are 0.339–0.678 m and 0.333–0.667 m, respectively.

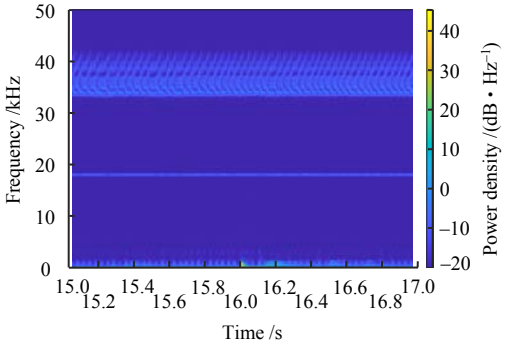

Fig. 8 Original signal spectrogram of data 1-1-15-1-1

4.2.3 Power density spectrum analysis

The power density spectrum of original signal of data 1-1-15-1-1 is presented in Fig.9. The low-frequency band is found to vibrate violently, which is consistent with the characteristics of the microseismic signal arrival. What's more, there are sudden changes in power when the frequency is around 18 kHz and 33 kHz for the high-frequency band. However, these changes are stable throughout the range, which does not meet the characteristics of the microseismic signal arrival.

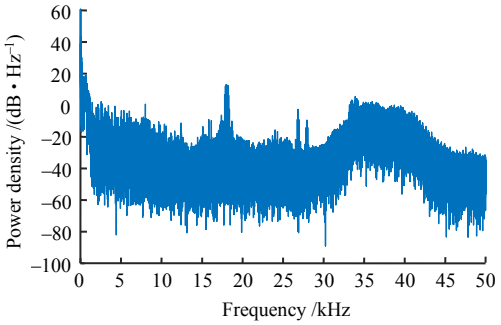

Fig. 9 Power density spectrum of original signal of data 1-1-15-1-1

4.2.4 Two successive band-pass filterings

(1) Rough filtering: The lower limit of the rough filtering is determined as 390.72 Hz using the corresponding method, and the upper limit is set as 1 kHz. The effect of the rough filtering is shown in Figs.10 and 11.

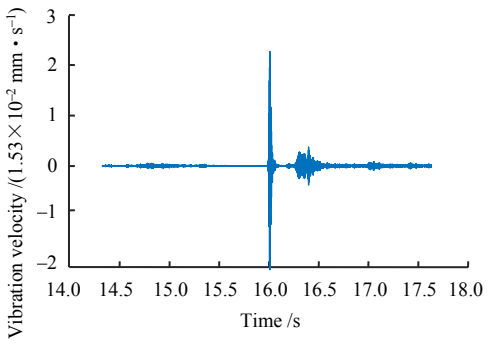

Fig. 10 Signal diagram of data 1-1-15-1-1 after rough filtering

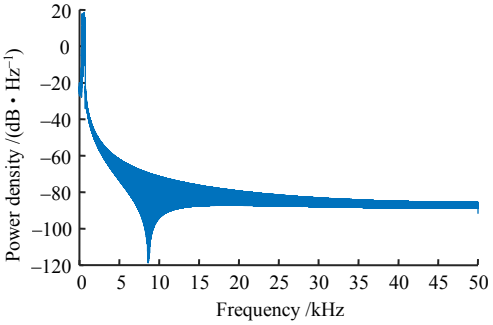

Fig. 11 Power density spectrum of data 1-1-15-1-1 after rough filtering

(2) Accurate filtering: Based on the calculation, the frequency corresponding to the maximum power is 598.85 Hz and it is the dominant frequency of S-wave, which is selected as the origin of the accurate band-pass filtering. As shown in Fig.8, the dominant frequency of P-wave in this test is about 590 Hz, and the difference between the two dominant frequencies is within 10 Hz. The radius of the accurate filtering R is set as 1 Hz for band-pass filtering, and its effect is shown in Fig.12.

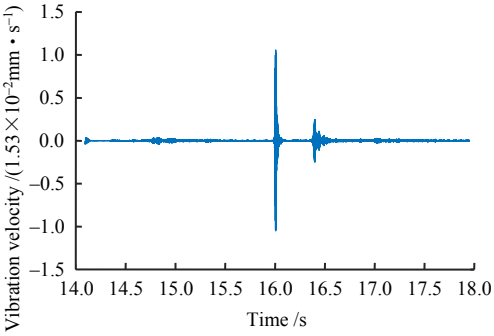

Fig. 12 Signal diagram of data 1-1-15-1-1 after accurate filtering

4.2.5 Arrival-time picking of the peak value of S-wave

According to the above analysis, the time corresponding to the maximum amplitude in Fig.12 is the peak arrival time of S-wave. The amplitudes of all data are sorted, and the maximum value can be observed when the S-wave peak arrival time is reached. The picking effect is shown in Fig.13.

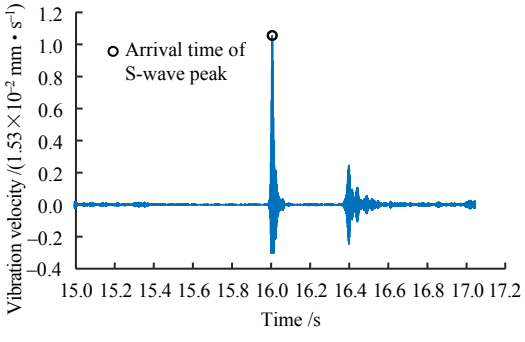

Fig. 13 Arrival-time picking of the peak value of S-wave

4.2.6 Accurate arrival-time picking of P-wave

By checking from the amplitude corresponding to the determined peak arrival time of S-wave to its left, the time corresponding to the amplitude of the wavelet that first deviates from the background noise is the accurate arrival time of P-wave. The data are processed by the TFA-DC method and the picking effect of the arrival time of P-wave is shown in Fig.14.

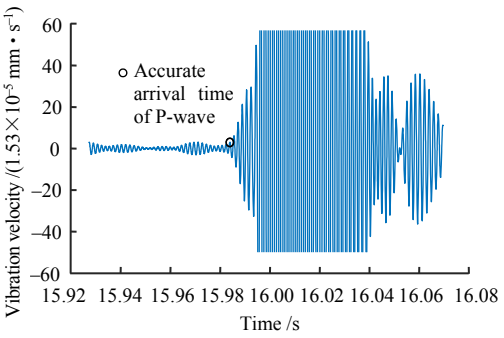

Fig. 14 Accurate arrival-time picking of P-wave

5 Accuracy analysis of the TFA-DC method

By sorting out all data, 576 sets of data are obtained in total. Two FIR band-pass filterings are performed on 32 sets of data selected in a certain order and the arrival time of the microseismic signals after the filtering is picked. In this article, the picking result of the manual picking method is taken as a standard, the advantages of the TFA-DC method in terms of calculation speed, accuracy and stability of picking results, adaptability of the signal with a low signal-to-noise ratio are verified by comparing arrival time picking results of the TFA-DC method and the improved STA/LTA method. The following principles are adopted in the manual picking method: the time corresponding to the maximum point of the amplitude of the full data is selected as the arrival time of S-wave peak; the time corresponding to the amplitude of the wavelet on the left side of S-wave peak that first deviates from the background noise is the accurate arrival time of P-wave. The processor Intel(R) Xeon CPU E3-1230 V2 @ 3.30 GHz with the memory of dual-channel Kingston DDDR-III 8 G 1 600 MHz is used for calculation.

5.1 Data analysis of the improved STA/LTA method

The STA/LTA method is a common method for picking up the arrival time of microseismic signals, which can accurately pick up P-wave in microseismic monitoring.

LTA represents the changing trend of signal background noise, and STA represents the changing trend of amplitude caused by the arrival of effective microseismic signals[22]. The basic formulas of the general STL/LTA method are[23]

$$\mathrm{LTA}(m)=\frac{1}{\mathrm{long}}\sum_{j=m}^{m+\mathrm{long}}\mathrm{CF}(j) \tag{6}$$

$$\mathrm{STA}(m)=\frac{1}{\mathrm{short}}\sum_{j=m+\mathrm{long}}^{m+\mathrm{long}+\mathrm{short}}\mathrm{CF}(j) \tag{7}$$

$$\frac{\mathrm{STA}}{\mathrm{LTA}}(m)=\frac{\mathrm{STA}(m)}{\mathrm{LTA}(m)}\geqslant\lambda \tag{8}$$

where m is the sample time (s); long is the length of the long time window (s); short is the length of the short time window (s); λ is set as the trigger threshold; and CF(j) is the corresponding characteristic function value of the microseismic signal at time j.

The selected characteristic function is the superposition of the absolute value of the amplitude of the microseismic record in the time window[24], namely

$$\mathrm{LTA}(m)=\frac{1}{\mathrm{long}}\sum_{j=m}^{m+\mathrm{long}}\left|A(j)\right| \tag{9}$$

$$\mathrm{STA}(m)=\frac{1}{\mathrm{short}}\sum_{j=m+\mathrm{long}}^{m+\mathrm{long}+\mathrm{short}}\left|A(j)\right| \tag{10}$$

$$\frac{\mathrm{STA}}{\mathrm{LTA}}(m)=\frac{\mathrm{STA}(m)}{\mathrm{LTA}(m)}\geqslant\lambda \tag{11}$$

where $\left|A(j)\right|$ is the absolute value of the amplitude of the microseismic record at time j.

Generally, a higher signal-to-noise ratio is required in the STA/LTA method. However, the low-frequency background noise has a greater impact in this test, so the rate and accuracy of the arrival time picking of P-wave are both low. Therefore, an improved STA/LTA method can be obtained by combining the rough filtering method and the general STA/LTA method. In this method, the original signal is first processed using the rough filtering, and then the arrival time of P-wave is accurately picked up according to the general STA/LTA method.

The improved STA/LTA method and manual picking method are both used to pick up the accurate arrival time of P-waves based on the above 32 sets of data. The sample interval is set as 10, the short-time window is set as 50 ms, the long-time window is set as 500 ms, and the trigger threshold is set as 5 in calculation. The results are listed in Table 2.

Table 2 Analysis of arrival-time picking results using improved STA / LTA method

Data No.	First impact of pendulum				Second impact of pendulum				Third impact of pendulum			
	Arrival time of manual picking /s	Accurate arrival time of P-wave /s	Time difference /s	Calculation time /s	Arrival time of manual picking /s	Accurate arrival time of P-wave s	Time difference /s	Calculation time /s	Arrival time of manual picking /s	Accurate arrival time of P-wave /s	Time difference /s	Calculation time /s
1-1-15-1	15.984 161	15.984 430	0.000 269	3.197 450	19.866 033	19.848 754	–0.017 279	3.208 801	23.225 988	23.210 824	–0.015 164	2.903 314
1-1-25-1	2.745 209	2.726 376	–0.018 833	2.850 259	7.621 346	7.606 265	–0.015 081	3.916 099	11.108 918	11.089 140	–0.019 778	3.059 957
1-1-15-2	15.974 484	—	—	4.717 611	19.864 291	19.849 986	–0.014 305	3.238 091	23.213 096	23.208 652	–0.004 444	2.951 472
1-1-25-2	2.744 949	2.765 442	0.020 493	2.782 720	7.621 516	2.723 372	–4.898 144	4.016 908	11.108 097	7.602 506	–3.505 591	3.179 432
1-3-15-3	5.193 587	—	—	5.432 198	10.210 445	—	—	4.724 175	13.347 862	13.346 580	–0.001 282	3.300 991
1-3-25-3	11.321 371	7.620 071	–3.701 300	0.994 191	15.028 707	15.011 117	–0.017 590	3.644 008	26.889 432	25.652 518	–1.236 914	7.333 608
1-3-15-4	4.941 082	—	—	5.379 837	10.205 711	—	—	4.715 806	13.297 693	—	—	5.505 735
1-3-25-4	11.334 443	—	—	7.502 882	15.038 811	—	—	10.395 543	26.908 431	—	—	9.653 793
2-2-10-7	5.644 298	5.626 425	–0.017 873	2.630 225	10.875 319	10.859 648	–0.015 671	4.146 887	13.528 605	14.150 453	0.621 848	3.265 045
2-2-20-7	3.847 009	3.827 082	–0.019 927	2.008 282	7.655 679	7.634 489	–0.021 190	3.135 367	11.242 234	11.22 341	–0.018 824	3.100 098
2-2-10-8	5.682 818	5.622 733	–0.060 085	2.646 588	10.867 968	10.860 048	–0.007 920	4.177 063	13.518 893	13.524 600	0.005 707	2.467 440
2-2-20-8	3.840 184	3.827 281	–0.012 903	2.021 320	7.646 231	7.635 038	–0.011 193	3.173 586	11.236 407	11.223 930	–0.012 477	3.123 012
2-4-10-9	4.528 233	4.512 949	–0.015 284	2.448 119	6.744 266	6.734 659	–0.009 607	1.985 261	8.971 672	8.962 611	–0.009 061	2.168 879
2-4-20-9	7.692 333	4.854 253	–2.838 080	4.857 275	10.066 407	10.050 219	–0.016 188	2.089 379	12.528 443	12.507 622	–0.020 821	2.334 618
2-4-10-10	4.534 849	4.520 356	–0.014 493	2.431 820	6.750 784	6.741 107	–0.009 677	1.996 513	8.976 066	8.974 835	–0.001 231	2.134 495
2-4-20-10	7.702 383	4.859 042	–2.843 341	4.718 465	10.071 763	10.057 056	–0.014 707	2.088 030	12.531 976	12.514 849	–0.017 127	2.294 917
3-1-15-1	7.361 014	7.338 576	–0.022 438	3.142 820	13.456 227	10.671 279	–2.784 948	1.195 047	18.325 323	18.303 691	–0.021 632	3.990 466
3-1-25-1	3.729 196	3.708 135	–0.021 061	2.377 077	6.459 437	6.435 238	–0.024 199	2.389 568	10.152 859	10.130 788	–0.022 071	3.279 257
3-1-15-2	7.356 781	7.330 969	–0.025 812	3.146 143	13.452 112	10.652 952	–2.799 160	1.203 524	18.320 638	18.295 794	–0.024 844	3.972 055
3-1-25-2	3.725 543	3.699 727	–0.025 816	2.421 959	6.454 149	6.427 971	–0.026 178	2.448 539	10.148 165	10.122 039	–0.026 126	3.294 262
3-3-15-3	4.589 771	4.572 074	–0.017 697	2.029 804	7.044 320	7.025 880	–0.018 440	2.200 385	9.261 163	9.245 926	–0.015 237	2.092 523
3-3-25-3	4.117 330	4.097 236	–0.020 094	3.670 442	6.571 738	6.550 928	–0.020 810	2.201 009	8.980 180	8.958 428	–0.021 752	2.217 986
3-3-15-4	4.601 947	—	—	2.568 189	7.052 688	—	—	2.599 036	9.269 146	—	—	3.952 305
3-3-25-4	4.123 565	—	—	4.783 377	6.580 869	—	—	2.751 150	8.989 513	—	—	4.051 853
4-2-10-7	3.683 982	3.659 892	–0.024 090	2.547 040	5.932 081	5.909 728	–0.022 353	1.992 130	8.017 633	7.995 539	–0.022 094	1.956 128
4-2-20-7	5.846 940	5.825 740	–0.021 200	6.588 543	8.417 512	8.396 670	–0.020 842	2.244 708	11.149 419	11.126 669	–0.022 750	2.556 351
4-2-10-8	3.681 557	3.659 393	–0.022 164	2.512 842	5.925 465	5.909 797	–0.015 668	1.997 536	8.017 693	7.994 172	–0.023 521	2.023 870
4-2-20-8	5.842 849	5.826 458	–0.016 391	6.667 192	8.412 373	8.399 660	–0.012 713	2.298 814	11.151 812	11.127 329	–0.024 483	2.513 492
4-4-10-9	17.633 150	17.625 172	–0.007 978	5.226 378	19.875 438	19.871 084	–0.004 354	2.049 705	21.862 489	21.851 368	–0.011 121	1.945 658
4-4-20-9	6.423 740	6.412 410	–0.011 330	4.567 197	9.839 388	9.830 843	–0.008 545	2.870 961	13.577 161	13.566 734	–0.010 427	3.260 360
4-4-10-10	17.632 449	17.625 473	–0.006 976	5.233 513	19.885 016	19.871 404	–0.013 612	1.993 298	21.869 105	21.855 592	–0.013 513	1.973 750
4-4-20-10	6.425 752	6.418 015	–0.007 737	4.555 342	9.840 489	9.832 952	–0.007 537	2.921 525	13.579 177	13.572 222	–0.006 955	3.247 545

According to Table 2, the following conclusions can be obtained:

(1) The maximum time difference of the accurate arrival time of P-wave is 4.898 144 s, the minimum time difference is 0.000 269 s, the average time difference is 0.326 153 s, and the standard deviation of the time difference is 0.968 478 s.

(2) The longest computational time is 10.395 543 s, the shortest computational time is 0.994 191 s, the average computational time is 3.330 940 s, and the standard deviation of computational time is 1.623 624 s.

(3) There are 15 picking failures caused by low

signal-to-noise ratio among the above picking results, accounting for 15.63%.

5.2 Data analysis of TFA-DC method

The TFA/DC method and manual picking method are both used to pick up the accurate arrival time of P-wave and arrival time of the peak value of S-wave based on the above 32 sets of data, as summarized in Table 3.

According to Table 3, the following results can be obtained:

(1) The maximum time difference, the minimum time difference, the average time difference and the standard deviation of S wave peak arrival time are all 0 s.

(2) The maximum time difference, the minimum time difference, the average time difference, and the standard deviation of the time difference of the accurate arrival time of P-wave are 0.014 759 s, 0 s, 0.002 014 s, and 0.003 859 s, respectively.

(3) The longest computational time is 1.922 409 s, the shortest computational time is 1.160 644 s, the average computational time is 0.171 069 s, and the standard deviation of the computational time is 0.171 069 s.

(4) There is no picking failure due to low signal-to-noise ratio among the above picking results.

Table 3 Analysis of arrival-time picking results using TFA-DC method

Data No.	First impact of the pendulum					Second impact of the pendulum of the pendulum					Third impact of the pendulum				
	Accurate arrival time of P-wave /s	Time difference /s	Arrival time of S-wave peak /s	Time difference /s	Calculation time /s	Accurate arrival time of P-wave /s	Time difference /s	Arrival time of S-wave peak /s	Time difference /s	Calculation time /s	Accurate arrival time of P-wave /s	Time difference /s	Arrival time of S-wave peak /s	Time difference /s	Calculation time /s
1-1-15-1	15.985 738	0.001 577	16.011 308	0	1.498 514	19.866 033	0.000 000	19.889 393	0	1.377 753	23.225 988	0.000 000	23.249 201	0	1.413 623
1-1-25-1	2.745 209	0.000 000	2.770 311	0	1.509 753	7.621 346	0.000 000	7.645 937	0	1.424 939	11.108 918	0.000 000	11.133 582	0	1.531 932
1-1-15-2	15.974 484	0.000 000	16.001 806	0	1.637 692	19.864 291	0.000 000	19.884 549	0	1.294 917	23.213 096	0.000 000	23.249 752	0	1.431 624
1-1-25-2	2.744 949	0.000 000	2.765 442	0	1.425 788	7.621 516	0.000 000	7.641 067	0	1.393 051	11.108 097	0.000 000	11.128 687	0	1.610 785
1-3-15-3	5.195 002	0.001 415	5.241 821	0	1.408 465	10.215 390	0.004 945	10.228 965	0	1.392 705	13.347 862	0.000 000	13.391 824	0	1.452 182
1-3-25-3	11.321 371	0.000 000	11.341 550	0	1.517 115	15.028 707	0.000 000	15.051 122	0	1.848 237	26.889 432	0.000 000	26.918 900	0	1.802 913
1-3-15-4	4.945 706	0.004 624	4.962 757	0	1.440 628	10.208 845	0.003 134	10.232 572	0	1.503 025	13.301 336	0.003 643	13.312 106	0	1.512 896
1-3-25-4	11.336 323	0.001 880	11.344 511	0	1.764 195	15.038 811	0.000 000	15.054 985	0	1.823 558	26.908 431	0.000 000	26.929 677	0	1.922 409
2-2-10-7	5.644 298	0.000 000	5.667 602	0	1.463 143	10.875 319	0.000 000	10.906 859	0	1.513 148	13.530 017	0.001 412	13.549 721	0	1.398 382
2-2-20-7	3.848 995	0.001 986	3.874 573	0	1.217 132	7.655 679	0.000 000	7.681 265	0	1.422 730	11.242 234	0.000 000	11.270 829	0	1.520 783
2-2-10-8	5.682 818	0.000 000	6.743 083	0	1.542 271	10.880 789	0.012 821	10.896 209	0	1.613 990	13.518 893	0.000 000	13.552 164	0	1.572 165
2-2-20-8	3.851 880	0.011 696	3.867 426	0	1.485 306	7.646 231	0.000 000	7.675 770	0	1.616 323	11.236 407	0.000 000	11.263 768	0	1.763 308
2-4-10-9	4.539 663	0.011 430	4.551 213	0	1.372 847	6.746 137	0.001 871	6.776 529	0	1.364 433	8.971 672	0.000 000	8.998 717	0	1.549 231
2-4-20-9	7.692 333	0.000 000	7.720 561	0	1.310 433	10.066 407	0.000 000	10.089 338	0	1.283 872	12.529 784	0.001 341	12.552 006	0	1.501 804
2-4-10-10	4.534 849	0.000 000	4.556 959	0	1.286 078	6.752 565	0.001 781	6.781 157	0	1.203 739	8.982 452	0.006 386	8.996 685	0	1.824 442
2-4-20-10	7.702 383	0.000 000	7.724 265	0	1.859 455	10.071 763	0.000 000	10.095 128	0	1.245 148	12.531 976	0.000 000	12.557 765	0	1.453 254
3-1-15-1	7.361 014	0.000 000	7.380 782	0	1.375 470	13.456 227	0.000 000	13.475 026	0	1.511 964	18.325 323	0.000 000	18.343 602	0	1.422 892
3-1-25-1	3.729 196	0.000 000	3.747 414	0	1.410 715	6.459 437	0.000 000	6.478 955	0	1.236 197	10.152 859	0.000 000	10.171 146	0	1.335 898
3-1-15-2	7.356 781	0.000 000	7.378 157	0	1.527 450	13.452 112	0.000 000	13.472 384	0	1.556 733	18.320 638	0.000 000	18.340 989	0	1.432 002
3-1-25-2	3.725 543	0.000 000	3.746 112	0	1.246 486	6.454 149	0.000 000	6.474961	0	1.278 405	10.148 165	0.000 000	10.168 504	0	1.488 965
3-3-15-3	4.591 807	0.002 036	4.609 352	0	1.202 189	7.044 320	0.000 000	7.062997	0	1.163 224	9.261 163	0.000 000	9.289 655	0	1.538 373
3-3-25-3	4.117 330	0.000 000	4.135 895	0	1.377 772	6.571 738	0.000 000	6.592 704	0	1.428 720	8.981 683	0.001 503	9.002 665	0	1.367 628
3-3-15-4	4.594 472	−0.007 475	4.619 701	0	1.259 239	7.052 688	0.000 000	7.073 347	0	1.312 447	9.269 146	0.000 000	9.290 585	0	1.395 147
3-3-25-4	4.125 169	0.001 604	4.144 328	0	1.427 757	6.580 869	0.000 000	6.601 462	0	1.241 931	8.991 317	0.001 804	9.011 447	0	1.435 369
4-2-10-7	3.694 871	0.010 889	3.709 646	0	1.250 114	5.943 236	0.011 155	5.958 110	0	1.160 644	8.017 633	0.000 000	8.043 042	0	1.362 075
4-2-20-7	5.846 940	0.000 000	5.869 139	0	1.636 618	8.417 512	0.000 000	8.443 369	0	1.358 691	11.149 419	0.000 000	11.173 003	0	1.435 235
4-2-10-8	3.681 557	0.000 000	3.704 992	0	1.353 004	5.940 224	0.014 759	5.955 648	0	1.415 247	8.017 693	0.000 000	8.038 117	0	1.306 384
4-2-20-8	5.842 849	0.000 000	5.868 358	0	1.868 407	8.412 373	0.000 000	8.438 697	0	1.499 290	11.151 812	0.000 000	11.171 151	0	1.324 612
4-4-10-9	17.633 150	0.000 000	17.670 526	0	1.742 180	19.886 227	0.010 789	19.905 994	0	1.285 417	21.873 159	0.010 670	21.891 026	0	1.447 733
4-4-20-9	6.435 331	0.011 591	6.453 484	0	1.624 422	9.839 388	0.000 000	9.870 378	0	1.397 370	13.577 161	0.000 000	13.609 719	0	1.646 481
4-4-10-10	17.642 649	0.010 200	17.672988	0	1.564 648	19.885 016	0.000 000	19.909 117	0	1.294 852	21.869 105	0.000 000	21.903 037	0	1.546 694
4-4-20-10	6.434 403	0.008 651	6.466 008	0	1.666 174	9.849 347	0.008 858	9.881 079	0	1.473 926	13.588 636	0.009 459	13.620 410	0	1.722 528

5.3 Comparison between the improved STA/LTA method and the TFA/DC method

Table 4 shows the comparison between the TFA-DC method and the improved STA/LTA for the arrival-time picking. Some conclusions can be made:

(1) The improved STA/LTA method can't identify the arrival time of the S-wave peak, while the TFA-DC method can accurately identify the arrival time of the S-wave peak and the average time difference can reach zero.

(2) The average time difference of the accurate arrival time of P-wave obtained by the TFA/DC method is 6.18‰ of that obtained by the improved STA/LTA method.

(3) The standard deviation of the time difference of the accurate arrival time of P-wave obtained by the TFA/DC method is 3.98‰ of that obtained by the improved STA/LTA method.

(4) The average computational time required by the TFA-DC method for a single picking is 43.99% of that of the improved STA/LTA method.

(5) The standard deviation of computational time required by the TFA-DC method for a single picking is 10.54% of that of the improved STA/LTA method.

(6) There is no picking failure of the accurate arrival time of P-wave and the arrival time of S-wave peak in the TFA-DC method. However, the picking failure of the accurate arrival time of P-wave accounts for 15.63%

in the improved STA/LTA method, indicating that the improved STA/LTA method has a poor adaptability in analysis of data with low signal-to-noise ratio compared to the TFA-DC method.

Table 4 Comparison between TFA-DC and improved STA / LTA

Method	Type of wave that can be picked up	Average time difference of arrival time of S-wave peak /s	Standard deviation of time difference of arrival time of S-wave peak	Average time difference of accurate arrival time of P-wave /s	Standard deviation of time difference of accurate arrival time of P-wave	Required calculation time for a single picking /s	Standard deviation of required calculation time for a single picking	Zero time difference (Yes or No)	Proportion of picking failures /%
TFA-DC	P-wave, S-wave	0	0	0.002 014	0.003 859	1.465 394	0.171 069	Yes	0.00
Improved STA/LTA	P-wave	Cannot pick	Cannot pick	0.326 153	0.968 478	3.330 940	1.623 624	No	15.63

6 Engineering verification

In order to further verify the reliability of the TFA-DC method for picking up the arrival time of microseismic signals, the microseismic signal data in the project of the Hongyang third coal mine is selected and the results are shown in Table 5.

Based on Table 5, some conclusions can be made:

(1) The maximum time difference, minimum time difference, average time difference and standard deviation of time difference of the arrival time of S-wave peak are all 0 s.

(2) For the accurate arrival time of P-wave, the maximum time difference is 0.025 380 s, the minimum time difference is 0 s, the average time difference is 0.007 825 s and the standard deviation of the time difference is 0.006 180 s.

(3) The longest computational time is 2.220 169 s, the shortest computational time is 1.418 231 s, the average computational time is 1.853 774 s, and the standard deviation of computational time is 0.220 383 s.

(4) There is no picking failure of the arrival time in the above results caused by low signal-to-noise ratio.

Based on the above results, it can be concluded that the TFA-DC method has certain advantages for the onsite arrival-time picking in terms of the types of waves that can be picked up, the average time difference, the standard deviation of the time difference, the average computational time required for a single picking, the standard deviation of the time, and the success rate of arrival-time picking. Therefore, this method is an effective method for picking up the arrival time of microseismic signals, which can also meet requirements of the project site.

Table 5 Analysis of arrival-time picking results of data from Hongyang third coal mine by TFA-DC

Data No.	Arrival of the first microseismic signal					Arrival of the second microseismic signal					Arrival of the third microseismic signal				
	Arrival time of P-wave /s	Time difference /s	Arrival time of S-wave /s	Time difference /s	Calculation time/s	Arrival time of P-wave /s	Time difference /s	Arrival time of S-wave /s	Time difference /s	Calculation time/s	Arrival time of P-wave /s	Time difference /s	Arrival time of S-wave /s	Time difference /s	Calculation time/s
Haozitun S-1	33.3444 53	0.011 880	35.305 053	0	1.992 557	33.950 253	0.012 670	35.246 253	0	1.897 983	33.568 053	0.016 910	35.190 653	0	1.618 210
Yangdianzi T-2	34.224 327	0.000 000	35.732 327	0	2.156 874	34.226 727	0.010 190	35.623 527	0	1.777 926	33.824 927	0.000 000	35.014 727	0	1.418 231
Shubeizi U-3	34.632 081	−0.006 050	36.495 281	0	1.985 086	34.550 881	−0.004 420	35.877 881	0	2.125 512	34.053 081	0.004 350	35.347 081	0	1.906 152
Beiqingdui W-4	34.237 030	0.009 470	36.076 430	0	1.852 137	34.488 830	0.006 880	35.431 230	0	1.622 768	33.906 830	0.000 000	35.519 830	0	2.188 781
Kuangchedui X-5	34.584 766	0.008 400	36.029 166	0	1.663 114	34.266 566	0.011 120	35.855 966	0	1.914 234	34.128 766	0.008 280	35.199 966	0	2.220 169
Huoyaoku Y-6	34.172 283	0.010 840	35.612 083	0	1.895 993	34.271 683	0.025 380	35.688 083	0	1.598 075	33.776 083	0.000 000	35.781 683	0	1.770 299
Gongyechang Z-7	34.378 501	−0.003 870	35.673 901	0	1.550 382	34.256 101	−0.004 150	35.360 701	0	1.836 228	34.097 501	−0.009 470	36.260 301	0	1.938 548

7 Conclusions

In this study, the TFA-DC method is developed based on the principles of time-frequency analysis and arrival-time picking. The accurate arrival time of P-wave and the arrival time of S-wave peak of the simulated microseismic signal are also picked up using the TFA-DC method and the improved STA/LTA method, respectively. In addition, the advantages of the TFA-DC method are determined using the manual picking result as the criterion, which is also verified in some projects. Some conclusions can be drawn as follows:

(1) The characteristics of microseismic signals can be determined by analyzing the spectrogram and power density spectrum. The position and law of the background noise can also be obtained to find the frequency, amplitude, and energy changes of the microseismic signal before and after the initial arrivals of P-wave and S-wave.

(2) After two successive FIR band-pass filterings, the rough filtering can filter out regular high-frequency and low-frequency background noise with power greater than that of P-wave and S-wave signals, and identify the dominant frequency of S-wave in the power density spectrum. The accurate filtering can filter out most of the unwanted signals and then only the signals within the accurate filtering radius are processed. Therefore, the required bandwidth can be accurately selected and the signal image is smoother, which is more suitable for iterative comparison.

(3) The TFA-DC method and the improved STA/LTA method are compared. The former method can pick up both the accurate arrival time of P-wave and the arrival time of S-wave peak value, while the latter can only pick up the accurate arrival time of P-wave. The average time difference and standard deviation of the accurate arrival time of P-wave obtained by the former are 6.18 ‰ and 3.98 ‰ of the latter, respectively. Additionally, the average computational time and standard deviation for a single picking of the former are 43.99% and 10.54% of the latter, respectively. The picking failure ratio of the former is 0, while that of the latter is 15.63%.

References

[1] PAN Yi-shan, ZHAO Yang-feng, GUAN Fu-hai, et al. Study on rockburst monitoring and orientation system and its application[J]. Chinese Journal of Rock Mechanics and Engineering, 2007, 26(5): 1002–1011.

[2] XU Nu-wen, LI Tao, DAI Feng, et al. Stability analysis on the left bank slope of Baihetan hydropower station based on discrete element simulation and microseismic monitoring[J]. Rock and Soil Mechanics, 2017, 38(8): 2358–2367.

[3] CUI Feng, YANG Yan-bin, LAI Xing-ping, et al. Similar material simulation experimental study on rockbursts induced by key stratum breaking based on microseismic monitoring[J]. Chinese Journal of Rock Mechanics and Engineering, 2019, 38(4): 803–814.

[4] LI Jin-yu, LEI Wen-jie, ZHAO Hong-bao, et al. Micro-seismic characteristics during impact failure of coal and rock under repetitive blast mining[J]. Journal of China University of Mining & Technology, 2019, 48(5): 966–974.

[5] WU Shun-chuan, CHEN Zi-jian, ZHANG Shi-huai, et al. Microseismic location algorithm for gently inclined strata and its numerical verification[J]. Rock and Soil Mechanics, 2018, 39(1): 297–307.

[6] JIA Bao-xin, WANG Kun, SUN Ao, et al. Experimental study on propagation law of microseismic signal in layered rock mass containing goaf[J]. Rock and Soil Mechanics, 2020, 41(10): 3255–3265.

[7] ZHANG Chu-xuan, LI Xi-bing, DONG Long-jun, et al. A S-wave phase picking method with four indicators of three functions for microseismic signal in mines[J]. Chinese Journal of Rock Mechanics and Engineering, 2015, 34(8): 1650–1659.

[8] ROSS Z E, MEIER M A, HAUKSSON E. P-wave arrival picking and first-motion polarity determination with deep learning[J]. Journal of Geophysical Research: Solid Earth, 2018, 123(6): 5120–5129.

[9] PEROL T, GHARBI M, DENOLLE M. Convolutional neural network for earthquake detection and location[J]. Science Advances, 2018, 4(2): e1700578.

[10] LEE M, BYUN J, KIM D, et al. Improved modified energy ratio method using a multi-window approach for accurate arrival picking[J]. Journal of Applied Geophysics, 2017, 139(1): 117–130.

[11] ZHU Meng-bo, WANG Li-guan, PENG Ping-an, et al. Modified PAI-k-MFV picker of picking microseismic P-wave arrival time and its application[J]. Journal of China Coal Society, 2017, 42(10): 2698–2705.

[12] JIA Rui-sheng, TAN Yun-liang, SUN Hong-mei, et al. Method of automatic detection on micro-seismic P-arrival time under low signal-to-noise ratio[J]. Journal of China Coal Society, 2015, 40(8): 1845–1852.

[13] DIEHL T, DEICHMANN N, KISSLING E, et al. Automatic S-wave picker for local earthquake tomography[J]. Crossref, 2009, 99(3): 1906–1920.

[14] ZHAO Da-peng, LIU Xi-qiang, LI Hong, et al. Detection of regional seismic events by Kurtosis method and automatic identification of direct P-wave first motion by Kurtosis-AIC method[J]. Journal of Seismological Research, 2012, 35(2): 220–225, 295.

[15] ZHANG H J, THURBER C, ROWE C A. Automatic P-wave arrival detection and picking with multiscale wavelet analysis for single-component recordings[J]. Bulletin of the Seismological Society of Americal, 2003, 93(5): 1904–1912.

[16] JIA Bao-xin, JIA Zhi-bo, ZHAO Pei, et al. Microseism location in local scale region based on high-density array[J]. Chinese Journal of Geotechnical Engineering, 2017, 39(4): 705–712.

[17] ZHAO Cong-cong, TANG Shao-hui, QIN Min, et al. Experimental study on positioning accuracy of micro-seismic monitoring system[J]. Mining Technology, 2019, 19(2): 46–49.

[18] ZHAO Shu-hong, WANG Xuan. Comparison between the time-frequency filtering of S transform method and other filter method[J]. Northwestern Seismological Journal, 2007, 29(3): 224–229.

[19] LU Cai-ping, DOU Lin-ming, WU Xing-rong, et al. Frequency spectrum analysis on microseismic monitoring and signal differentiation of rock material[J]. Chinese Journal of Geotechnical Engineering, 2005, 27(7): 772–775.

[20] XIAO Tian. Studies on the downhole microseismic monitoring methods[D]. Hefei: University of Science and Technology of China, 2018.

[21] LI Zhi-min, GOU Xian-tai, JIN Wei-dong, et al. Frequency features of microseismic signals[J]. Chinese Journal of Geotechnical Engineering, 2008, 187(6): 830–834.

[22] LIU Han, ZHANG Jian-zhong. STA/LTA algorithm analysis and improvement of microseismic signal automatic detection[J]. Progress in Geophysics, 2014, 29(4): 1708–1714.

[23] LIU Xiao-ming, ZHAO Jun-jie, WANG Yun-min, et al. Automatic picking of microseismic events P-wave arrivals based on improved method of STA/LTA[J]. Journal of Northeastern University (Natural Science), 2017, 38(5): 740–745.

[24] WU Zhi-tao, LI Shi-xiong. Comparison of STA/LTA P-pickers for micro seismic monitoring[J]. Progress in Geophysics, 2010, 25(5): 1577–1582.